

Femtosecond laser fabrication of nanopillar arrays for Surface-Enhanced Raman scattering substrates

Yunfang Zhang^{a,b}, Yubin Deng^{a,b}, Han Liu^{a,b}, Longbiao Huang^{a,b}, Xin Ding^{a,b}, Zhiyong Bai^{a,b}, Changrui Liao^{a,b}, Yiping Wang^{a,b}, Ying Wang^{a,b,*}

^a Shenzhen Key Laboratory of Ultrafast Laser Micro/Nano Manufacturing, Key Laboratory of Optoelectronic Devices and Systems of Ministry of Education/Guangdong Province, College of Physics and Optoelectronic Engineering, Shenzhen University, Shenzhen 518060, China

^b Shenzhen Key Laboratory of Photonic Devices and Sensing Systems for Internet of Things, Guangdong and Hong Kong Joint Research Centre for Optical Fibre Sensors, State Key Laboratory of Radio Frequency Heterogeneous Integration, Shenzhen University, Shenzhen 518060, China

ARTICLE INFO

Keywords:

Femtosecond laser fabrication
Two-photon polymerization technology
Nanopillar
Surface-enhanced Raman scattering

ABSTRACT

This work presents a femtosecond laser fabrication method for precision-engineered nanopillar arrays, applicable for surface-enhanced Raman scattering (SERS) substrates. The proposed method consists of two steps: (1) fabrication of nanopillar arrays using femtosecond laser-induced two-photon polymerization (TPP) technology; and (2) deposition of Ag nanoparticles on the fabricated nanopillar arrays. Nanopillar arrays of the proposed SERS substrates are optimized with geometrical parameters of diameter, height, spacing, and arrangement. A limit of detection (LOD) down to 10^{-7} mol/L for Rhodamine 6G solution is achieved and the enhancement factor is estimated to be up to 2×10^3 . The experimental results indicate that the proposed SERS substrates have potential applications in biomedical detection, food safety monitoring, and quality control.

1. Introduction

Raman spectroscopy is a powerful tool to determine the structure of chemicals by analyzing the vibrational and rotational energy levels of molecules, also known as a molecular “fingerprint” spectrum [1,2]. It has been widely used in non-destructive detection and molecular identification. However, Raman scattering is a fragile type of light-matter interaction with the signal generally only about 10^{-10} of the incident light intensity, which greatly limits practical applications. In 1974, Fleischmann et al. found that the Raman signal intensity between the adjacent molecules adsorbed on the surface of the rough Ag electrode was significantly enhanced, which was the first time that the Surface-enhanced Raman spectroscopy (SERS) effect was observed [3,4].

The intensity of a Raman signal is governed by the characteristics of the SERS active substrate. With the development of SERS substrate preparation technology, research interests are generally focused on regulating substrate structural parameters, including the morphology, size, and spatial arrangement of nanoparticles. With the continuous in-depth study of nanomaterials and their preparation technology, SERS substrates have been developed from the earliest unstable and rough

synthetic metal electrode to a repeatable and ordered metal structure. Nowadays, customizable metal-ordered SERS substrates have become a hot research topic for high-performance SERS active substrates.

Homogeneity is a crucial factor in evaluating SERS substrates, particularly when used for quantitative detection and imaging. Reliable detection outcomes depend on the reproducibility of the detection results from the substrate since SERS is a localized phenomenon that is highly sensitive to the local structure of the substrate and its surrounding environment. For nanoparticle-based substrates, homogeneity in size, shape, and aggregation state enhances the reproducibility. In the case of assembly- or array-based substrates, the controllable gap size and its distribution are pivotal [5]. Up to now, novel fabrication techniques of SERS substrates such as photolithography [6], electron-beam lithography [7–11] and focused ion beam milling (FIB) [12–16] have been extensively investigated to solve these problems. However, they still face challenges related to uniformity, efficiency, controllability, repeatability, and complexity in the fabrication process.

In this letter, we present a method for producing tailor-made and reproducible SERS substrates on a silica glass slide using femtosecond laser-induced two-photon polymerization (fs-TPP) and magnetron

* Corresponding author at: Shenzhen Key Laboratory of Ultrafast Laser Micro/Nano Manufacturing, Key Laboratory of Optoelectronic Devices and Systems of Ministry of Education/Guangdong Province, College of Physics and Optoelectronic Engineering, Shenzhen University, Shenzhen 518060, China.

E-mail address: yingwang@szu.edu.cn (Y. Wang).

<https://doi.org/10.1016/j.optlastec.2024.111659>

Received 23 April 2024; Received in revised form 14 August 2024; Accepted 19 August 2024

Available online 28 August 2024

0030-3992/© 2024 Elsevier Ltd. All rights reserved, including those for text and data mining, AI training, and similar technologies.

sputtering technology. Compared with the abovementioned lithography and FIB techniques, fs-TPP nanoprinting technology is based on layer-by-layer stacking manufacturing stacking, which greatly improves the flexibility and formation for micro-/nano-structure designs [17–21]. Here, the nanopillar arrays are initially fabricated on a planar glass slide, then Ag nanoparticles are sputtered onto the nanopillar arrays. The geometry parameters of the nanopillar arrays in proposed SERS substrates are optimized in terms of diameter, height, spacing, and arrangement [22]. Significant enhancement in the Raman signal is demonstrated by using the optimized SERS substrates for Rhodamine 6G detection.

2. Fabrication

Fig. 1 shows the schematic diagram of the proposed nanopillar array for SERS substrates, where the nanopillar array is fabricated by a femtosecond laser-based three-dimensional (3D) printing system. Femtosecond laser pulses with a central wavelength of 780 nm and a pulse duration of approximately 120 fs are focused onto the surface of a silica glass slide through a 63X objective lens with a numerical aperture (NA) of 1.40 and a working distance of 190 μm , which is immersed in the photo resin (IP-dip) that covering the glass slide. With this photo resin, a minimum feature size of about 300 nm can be readily achieved through the fs-TPP process. The geometry model of a nanopillar array like that shown in Fig. 1 can be drawn with CAD software and imported into the printing system. Before SERS substrate fabrication, the silica glass slide used here ($25 \times 25 \times 1.1 \text{ mm}^3$) undergoes a cleaning process with acetone, isopropyl alcohol (IPA), anhydrous ethanol, and deionized water (DIW) sequentially, followed by gently drying under a nitrogen gas stream. After the fs-TPP patterning of the nanopillar arrays, the samples are then immersed in propylene glycol methyl ether acetate (PGMEA) for 15-minute development, followed by another 5-minute immersion in IPA to completely remove the non-crosslinked residue.

Before fabricating nanopillar arrays, the fabrication parameters of a single nanopillar have been investigated for the consideration of stability, including diameter and height. Thin and long nanopillars are beneficial for the preparation of high-performance SERS substrates as they can effectively increase the specific surface area. As depicted in Fig. 2, nanopillars with diameters of 300 nm, 400 nm, 500 nm and, 600 nm are shown in columns (a) to (d), respectively, and the height of nanopillars in each column from top to bottom increases from 1 μm to 14 μm . It is evident that thicker nanopillars stand upright even with a height of 14 μm , such as that with a diameter of 500 nm and 600 nm, as

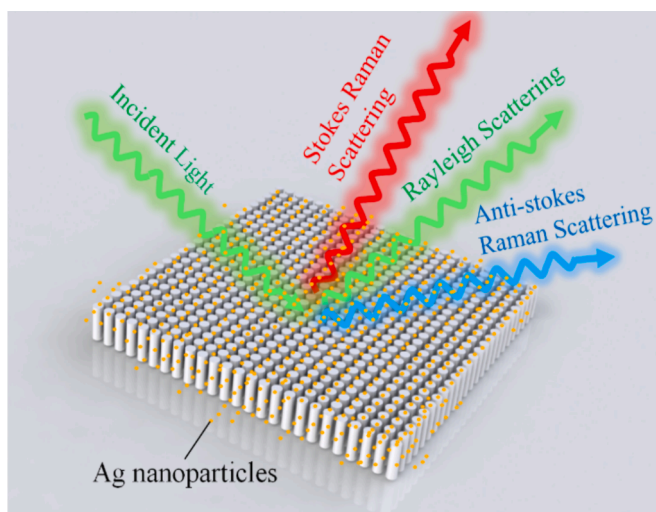


Fig. 1. Schematic diagram of Raman scattering enhancement generated by nanopillar arrays.

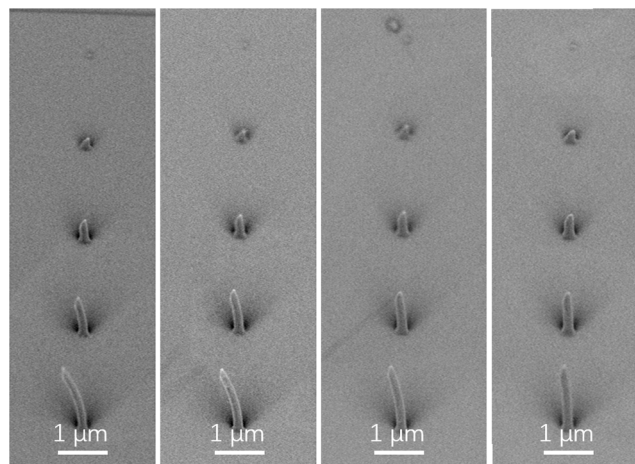


Fig. 2. Optimization and comparison of various nanopillars on a planar substrate. (a)–(d) The diameter of nanopillars are 300 nm, 400 nm, 500 nm, and 600 nm, respectively. From top to bottom, the height of nanopillars in each column is 1 μm , 3 μm , 6 μm , 10 μm , and 14 μm , respectively.

can be seen clearly from Fig. 2(c) and 2(d). The thinner ones are more prone to bending. For the nanopillars with a diameter of 300 nm, it can still stand upright with a height of 10 μm . However, a slight bent can be observed with the height increased to 14 μm , as shown in the bottom of Fig. 2(a). At this point, the aspect ratio reaches approximately 46.

In order to find the optimal close packing arrangement, we also investigated the arrangement effect of nanopillars. The fabricated nanopillar cells with different arrangements are shown in Fig. 3, which includes the basic triangular, quadrilateral, pentagonal and hexagonal arrangements. Note that the diameter and height of nanopillars here are all 300 nm and 10 μm , respectively. According to the scanning electron microscopy (SEM) images shown in Fig. 3(a), the critical distance (center to the vortex of the cell) for the non-tipping of the triangular arrangement nanopillar cell is determined to be 1.6 μm . Those for the quadrilateral, pentagonal, and hexagonal arrangements are 1.9 μm , 1.9 μm , and 2.3 μm , respectively. Therefore, the triangular arrangement of the nanopillar array exhibits the highest cover density under the same fabrication conditions, which is beneficial for SERS performance improvement. Moreover, the triangular arrangement is most stable under liquid tension.[23] Taking into account both the cover density and stability, the optimal arrangement can be determined to be the triangular one.

To explain the experimental results mentioned above, we conducted

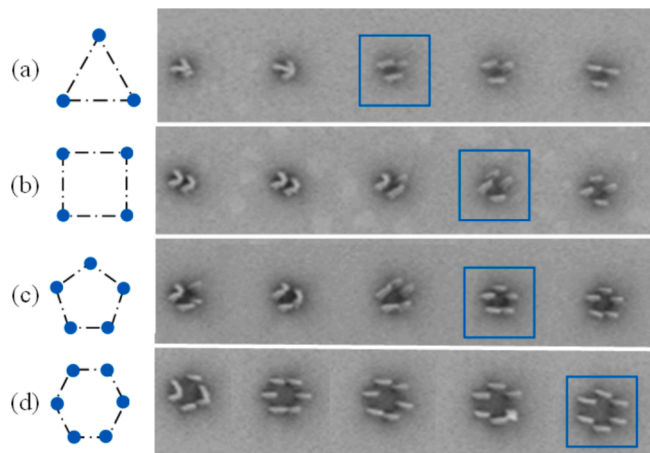


Fig. 3. SEM images of the morphology of the nanopillar arrays fabricated by fs-TPP with different arrangements.

mechanical simulations of the surface tension effect on the nanopillar with different heights and diameters. The simulation results are shown in Fig. 4, where one can see that when a nanopillar with the same radius is subjected to the same magnitude of surface tension, the top displacement of the nanopillar increases with its height. On the other hand, when a nanopillar with the same height is subjected to the same magnitude of surface tension, the top displacement of the nanopillar decreases with its radius increasing. As mentioned above, the critical distance of the triangular nanopillar array shown in Fig. 3 (a) is 1.6 μm , corresponding to a gap of $\sim 2.4 \mu\text{m}$ between adjacent nanopillars, which implies a non-tipping tolerance of 1.2 μm for the top displacement of nanopillars. According to the simulation results, the top displacement of a nanopillar with a diameter of 300 nm and a height of 10 μm is approximately 1.22 μm , as labeled by a red dot in Fig. 4, which is in good agreement with the experimental results. Due to the limitation of processing precision, the minimum diameter of a nanopillar is $\sim 300 \text{ nm}$. Therefore, the fabrication of short nanopillars is helpful to the realization of non-tipping nanopillar arrays. Meanwhile, it also reduces fabrication time.

3. Results and discussion

For the purpose of improving array density, the height of the printed nanopillar should be suppressed in cost. With a diameter of 300 nm and a height of 1 μm , the distance between adjacent nanopillars can be optimized down to submicron. Three nanopillar arrays with spacing distances of 700 nm, 800 nm, and 900 nm are shown in Fig. 5, respectively, where the fabricated nanopillar arrays are in good uniformity, as can be seen from the SEM images. Finally, the nanopillar arrays are coated with Ag nanoparticles using the magnetron sputtering method, as shown in Fig. 6 (a). The SEM images show that silver nanoparticles are evenly distributed on the surface of the nanopillars. We have statistically analyzed the size distribution of silver nanoparticles, the results of which are shown in Fig. 6 (b), and calculated the average diameter of the silver nanoparticles to be $\sim 10 \text{ nm}$. During sputtering, the vacuum chamber pressure is reduced to $5 \times 10^{-4} \text{ Pa}$, followed by continuous filling with argon at a quasi-static pressure of 2 Pa. The DC current intensity is set to 40 mA. To ensure the uniformity of the Ag nanoparticles, the nanopillar arrays are automatically rotated at a constant speed in the chamber during the sputtering process.

To evaluate the performance of the as-prepared SERS substrate, a Raman spectrometer (Alpha 300R, Witec) with a confocal microscope is

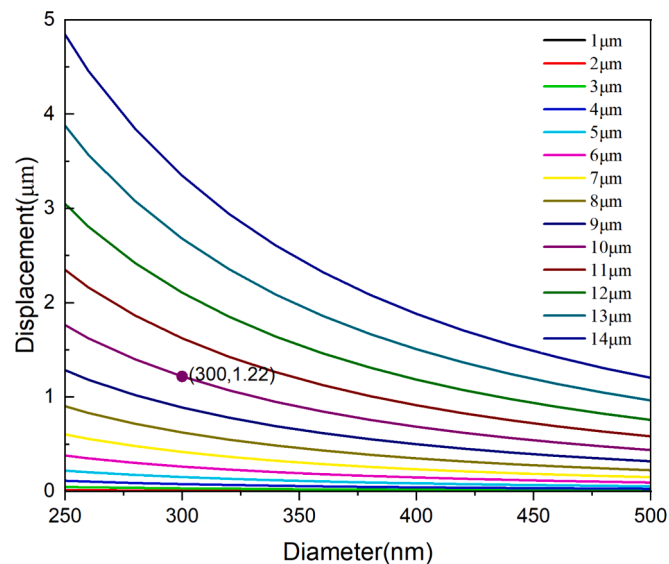


Fig. 4. Simulation of displacement induced by surface tension on nanopillars with different radii and heights.

used for Rhodamine 6G (R6G) detection, where a 532-nm frequency-stabilized single-mode diode laser is included for Raman signal excitation [24–26]. The sample is illuminated by a 532-nm laser beam with a power of 1 mW that is focused through a $100 \times$ microscopic objective (Olympus, 0.9NA) during the test. For data collection, the integration time and scan number for averaging are 1 s and 10, respectively. R6G aqueous solution is prepared by dissolving R6G powder in anhydrous ethanol. Serial dilutions are carried out to produce R6G solutions with concentrations ranging from 10^{-4} M to 10^{-8} M . The average thickness of R6G molecules on the surface of nanopillar array-based SERS substrate can be calculated through the relationship among concentration, solution volume, R6G density, and substrate area. For example, the volume of R6G solution used with a concentration of 10^{-5} mol/L (concentration units, where “mol” stands for the amount of substance in moles, and “L” stands for the volume in liters) is 10 μL during Raman test, and the area of the substrate is about 120 nm^2 , thus the average thickness of R6G powder after drying can be estimated to be 3 nm. This allows for the performance assessment and comparison of different SERS substrates.

Fig. 7 shows the Raman spectra of R6G with a concentration of 10^{-5} mol/L that corresponds to the SERS substrates with a nanopillar spacing of 700 nm, 800 nm, and 900 nm, respectively. Results indicate that the SERS substrate with a 900-nm spacing distance exhibits the highest intensity. This result is consistent with that of the previous report [5]. In order to further evaluate the performance of the proposed SERS substrates, we measured the Raman spectra of R6G with concentrations from 10^{-8} mol/L to 10^{-4} mol/L , as shown in Fig. 8(a). The Raman peak intensity with respect to the R6G concentration is plotted in semi-logarithmic scale, as can be seen in Fig. 8(b). Note that the data of 10^{-8} mol/L is not included in Fig. 8(b) due to the lack of identifiable Raman signals for this concentration. The Raman peak intensity rises as the concentration increases from 10^{-8} to 10^{-5} mol/L and approaches saturation at the concentration of 10^{-5} mol/L , and then drops with the R6G concentration further increases. On one hand, this is possibly due to the gaps between silver nanoparticles on the surface of nanopillar arrays being obscured by the overly thick layer of R6G molecules for high concentrations, leading to a weakening of the surface plasmon resonance (SPR) effect. In this case, the enhancement effect of the electromagnetic field is no longer significant, and the enhancement effect of the Raman signal will also be affected [21]. On the other hand, at high concentrations, R6G molecules may aggregate, affecting their adsorption state and orientation on the metal surface. This aggregation may reduce the number of molecules effectively adsorbed in the hot spot areas, thereby diminishing the enhancement effect of the Raman signal. The detection limit is estimated to be on the order of 10^{-7} mol/L .

The analytical enhancement factor (AEF) is an important indicator to characterize the SERS substrate. Note that the AEF does not fully encompass the SERS effect, as it disregards surface effects such as molecular coverage and surface adsorption. Therefore, it is influenced by the molecular species and the sample preparation process. Nevertheless, the AEF offers a straightforward figure for the expected signal enhancement in practical analytical measurements. The wavenumber and intensities of the major peaks are extracted from the baseline-corrected spectra and are used in the following equation [25,27]:

$$\text{AEF} = \frac{I_{\text{SERS}}}{I_{\text{RS}}} \cdot \frac{C_{\text{RS}}}{C_{\text{SERS}}} \quad (1)$$

where I_{SERS} and C_{SERS} denote the peak intensity and concentration of the analyte for SERS measurements, while I_{RS} and C_{RS} represent the equivalent values for non-SERS measurements. Additional measurement parameters, such as integration times, are taken into consideration to calculate normalized AEFs [28]:

$$\text{AEF}_{\text{nor}} = \frac{I_{\text{SERS}}}{I_{\text{RS}}} \cdot \frac{t_{\text{RS}}}{t_{\text{SERS}}} \cdot \frac{C_{\text{RS}}}{C_{\text{SERS}}} \quad (2)$$

where t_{SERS} and t_{RS} represent the integration times employed in the SERS

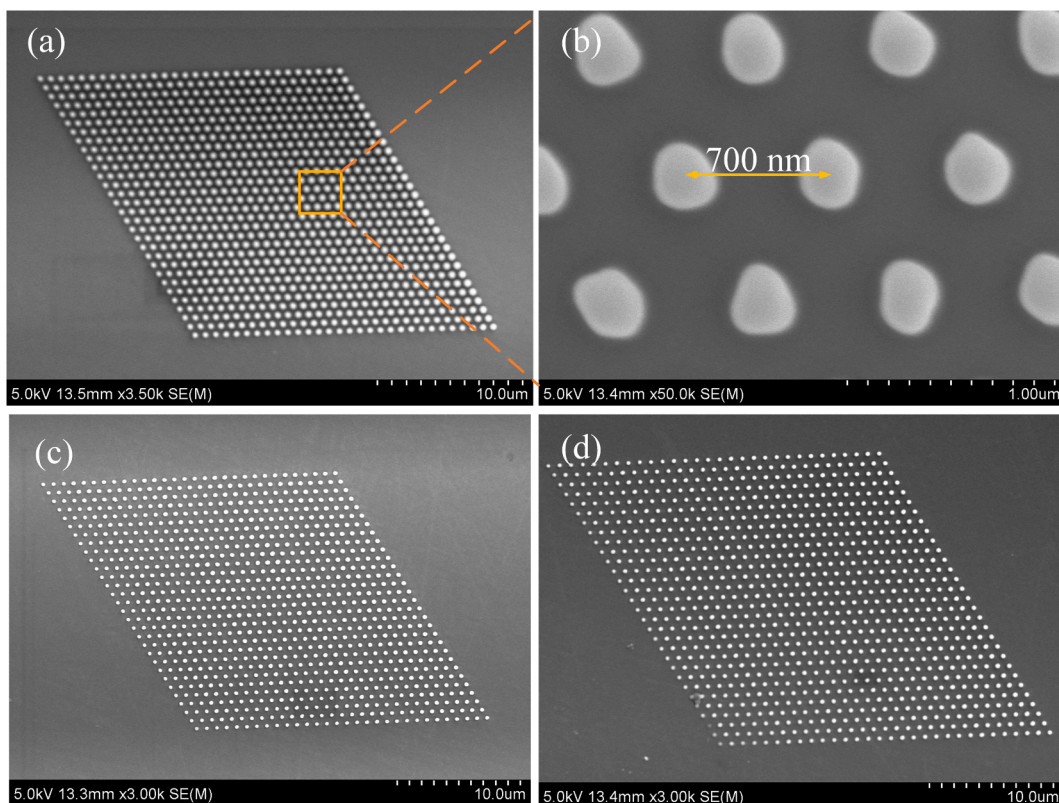


Fig. 5. SEM images of the morphology of the nanopillar arrays fabricated by fs-TPP with different spacing distances.

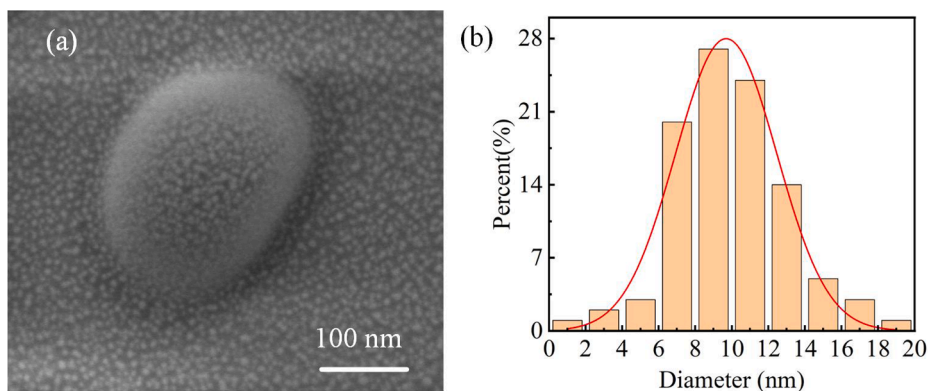


Fig. 6. (a) SEM images of the morphology of the Ag nanoparticles. (b) The particle size distribution of silver nanoparticles. Inset shows the Gaussian fit of the distribution. Fitting function: $y = 0.28\exp(-\ln(2)(2(x-9.6)/7.2)^2)$, where we can see, the mean value is 9.6 nm, the FWHM is 7.2 nm, and the amplitude is 28 %.

and non-SERS measurements, respectively. In cases where different laser powers, averaging values, and other parameters are utilized for SERS and non-SERS measurements, identical correction calculations are also conducted. For our experimental results, the normalized AEF value is calculated to be about 2×10^3 , and the detection limit is as low as 10^{-7} mol/L.

Table 1 lists the performance of the proposed SERS substrate and some typical fiber optic SERS substrates. Compared with the fiber optic SERS substrates, the LOD of the proposed SERS substrates for the R6G test reaches 10^{-7} mol/L, which is close to most methods in Table 1. The proposed method for SERS substrate fabrication is designable and reproducible, and there is still room for performance improvement in the future.

4. Conclusion

In conclusion, a method of fabricating precision-engineered and reproducible SERS substrates based on femtosecond laser-induced two-photon polymerization was proposed. The demonstrated SERS substrates were realized by nanopillar arrays made from femtosecond laser-induced two-photon polymerization and followed by the deposition of silver nanoparticles on the nanopillar arrays through magnetron sputtering. The geometrical parameters of the nanopillar array, including diameter, height, spacing, and arrangement, are optimized experimentally and a single nanopillar with an aspect ratio of 1:46 can be readily obtained. SERS substrates with optimized nanopillar arrays exhibit a limit of detection of 10^{-7} mol/L for the Rhodamine 6G test and achieve an analytical enhancement factor of approximately 2×10^3 . The proposed SERS substrate is expected to possess advantages in the fields of cost-effective biomedical detection and chemical sensing.

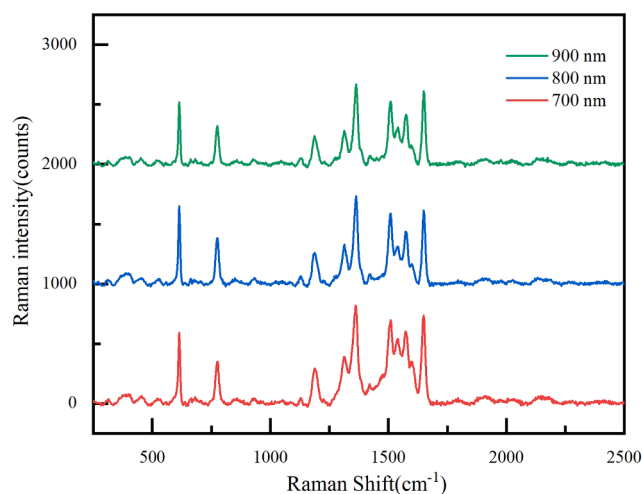


Fig. 7. SERS spectra for 10^{-5} mol/L R6G on silver nanopillar arrays substrates fabricated with different spacing distances. Spectrum offsets bottom-up are 0, 1000, and 2000 in counts, respectively.

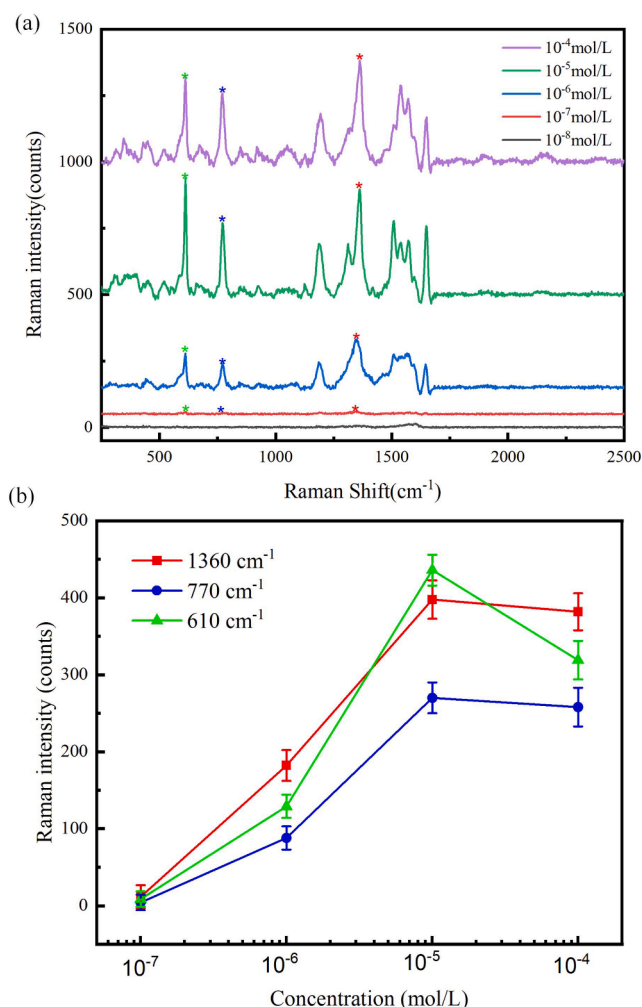


Fig. 8. (a) Spectra of R6G solution concentrations (R6G) ranging from 10^{-8} to 10^{-4} mol/L. Spectrum offsets bottom-up are 0, 100, 200, 500, and 1000 in counts, respectively. (b) The relationship between Raman spectral peak intensity and the R6G concentration at 1360 cm^{-1} , 770 cm^{-1} , and 610 cm^{-1} , respectively.

Table 1

Performance comparison with typical fiber-optic SERS substrates.

Type structures	Experimental methods	LOD (mol/L)	AEF	Ref
D-shaped fiber/Au Nanoparticles	Femtosecond laser ablation	10^{-7}	/	[29]
Fiber taper / Ag Nanoparticles	Chemical modification	10^{-7}	10^8	[30]
Fiber facet/Au Nanoparticles	Oil-water separation method	10^{-8}	/	[31]
Fiber facet nanopillars/Au film	Two-photon/3D printing	10^{-6}	1300	[5]
nano-pillars array/Ag Nanoparticles	Two-photon/3D printing	10^{-7}	2×10^3	This work

CRedit authorship contribution statement

Yunfang Zhang: Writing – original draft, Software, Methodology, Formal analysis, Conceptualization. **Yubin Deng:** Software, Formal analysis. **Han Liu:** Formal analysis. **Longbiao Huang:** Formal analysis, Conceptualization. **Xin Ding:** Software, Methodology. **Zhiyong Bai:** Writing – review & editing, Formal analysis. **Changrui Liao:** Supervision, Conceptualization. **Yiping Wang:** Writing – review & editing, Writing – original draft, Supervision, Formal analysis. **Ying Wang:** Writing – review & editing, Writing – original draft, Supervision, Formal analysis.

Declaration of competing interest

The authors declare that they have no known competing financial interests or personal relationships that could have appeared to influence the work reported in this paper.

Data availability

The data that has been used is confidential.

Acknowledgments

This work was supported by National Natural Science Foundation of China (62122057, 62275172); Guangdong Natural Science Foundation (2023A1515012893, 2022B1515120061); Shenzhen Key Laboratory of Ultrafast Laser Micro/Nano Manufacturing (ZDSYS202206061004 05013); Science and Technology Innovation Commission of Shenzhen (JCYJ20220818095615034); Shenzhen Science and Technology Program (KQTD20221101093605019).

References

- [1] Judith Langer, Dorleta Jimenez de Aberasturi, Javier Aizpurua, Ramon A. Alvarez-Puebla, Baptiste Auguie, Jeremy J. Baumberg, Guillermo C. Bazan, Steven E. J. Bell, Anja Boisen, Alexandre G. Brolo, Jaebum Choo, Dana Ciialla-May, Volker Deckert, Laura Fabris, Karen Faulds, F. Javier García de Abajo, Royston Goodacre, Duncan Graham, Amanda J. Haes, Christy L. Haynes, Christian Huck, Tamitake Itoh, Mikael Kall, Janina Kneipp, Nicholas A. Kotov, Hua Kuang, Eric C. Le Ru, Hiang Kwee Lee, Jian-Feng Li, Xing Yi Ling, Stefan A. Maier, Thomas Mayerhöfer, Martin Moskovits, Kei Murakoshi, Jwa-Min Nam, Shuming Nie, Yukihiko Ozaki, Isabel Pastoriza-Santos, Jorge Perez-Juste, Juergen Popp, Annemarie Pucci, Stephanie Reich, Bin Ren, George C. Schatz, Timur Shegai, Sebastian Schlücker, Li-Lin Tay, K. George Thomas, Zhong-Qun Tian, Richard P. Van Duyne, Tuan Vo-Dinh, Yue Wang, Katherine A. Willets, Chuanlai Xu, Hongxing Xu, Yikai Xu, Yuko S. Yamamoto, Bing Zhao, and Luis M. Liz-Marzán, Present and Future of Surface-Enhanced Raman Scattering, *ACS Nano* 14 (2020) 28–117.
- [2] D. Graham, M. Moskovits, Z.-Q. Tian, SERS – facts, figures and the future, *Chem. Soc. Rev.* 46 (2017) 3864–3865.
- [3] R. Pilot, R. Signorini, C. Durante, L. Orian, M. Bhamidipati, L. Fabris, A review on surface-enhanced Raman scattering, *Biosensors* 9 (2) (2019) 57.
- [4] M. Fleischmann, P.J. Hendra, A.J. McQuillan, Raman spectra of pyridine adsorbed at a silver electrode, *Chem. Phys. Lett.* 26 (2) (1974) 163–166.

- [5] Ah. Jang, D.J. Kim, A.J. Wales, G.-Z. Thompson, Fiber-Optic SERS Probes Fabricated Using Two-Photon Polymerization for Rapid Detection of Bacteria, *Adv. Opt. Mater.* 8 (9) (2020) 1901934.
- [6] Y. Zhao, Y.L. Zhang, J.A. Huang, Z. Zhang, X. Chen, W. Zhang, Plasmonic nanopillar array embedded microfluidic chips: an in situ SERS monitoring platform, *J. Mater. Chem. A* 3 (12) (2015) 6408–6413.
- [7] T. Duan, C. Gu, D.S. Ang, K. Xu, Z. Liu, A novel fabrication technique for high-aspect-ratio nanopillar arrays for SERS application, *RSC Adv.* 10 (2020) 45037.
- [8] L. Gutierrez-Rivera, R.F. Peters, S.K. Dew, M. Stepanova, Application of EBL fabricated nanostructured substrates for surface enhanced Raman spectroscopy detection of protein A in aqueous solution, *J. Vac. Sci. Technol. B* 31 (6) (2013).
- [9] R.F. Peters, L. Gutierrez-Rivera, S.K. Dew, M. Stepanova, Surface Enhanced Raman Spectroscopy Detection of Biomolecules Using EBL Fabricated Nanostructured Substrates, *JOVE-J vis Exp.* 97 (2015) e52712.
- [10] Neval A. Cinel, Semih Cakmakcayapan, Serkan Butun, Gulay Ertas, Ekmel Ozbay, E-Beam lithography designed substrates for surface enhanced Raman spectroscopy, *Photon. Nanostruct.* 15 (2015) 109–115.
- [11] N.A. Abu Hatab, J.M. Oran, M.J. Sepaniak, Surface-enhanced Raman spectroscopy substrates created via electron beam lithography and nanotransfer printing, *ACS Nano* 2 (2) (2008) 377–385.
- [12] Y.-Y. Lin, J.-D. Liao, Ju. Yu-Hung, C.-W. Chang, A.-L. Shiau, Focused ion beam-fabricated Au micro/nanostructures used as a surface enhanced Raman scattering-active substrate for trace detection of molecules and influenza virus, *Nanotechnology* 22 (2011) 185308.
- [13] T. Gao, Xu. Zongwei, F. Fang, W. Gao, Q. Zhang, Xu. Xiaoxuan, High performance surface-enhanced Raman scattering substrates of Si-based Au film developed by focused ion beam nanofabrication, *Nanoscale Res. Lett.* 7 (2012) 399.
- [14] A. Dhawan, M. Gerhold, T. Vo-Dinh, Theoretical Simulation and Focused Ion Beam Fabrication of Gold Nanostructures for Surface-Enhanced Raman Scattering (SERS), *Nanobiotechnology* 3 (2007) 164–171.
- [15] K. Sivashanmugan, J.-D. Liao, J.-W. You, Wu. Chao-Liang, Focused-ion-beam-fabricated Au/Ag multilayered nanorod array as SERS-active substrate for virus strain detection, *Sens. Actuators B Chem.* 81 (2013) 361–367.
- [16] J. Prakash, D.N. Samriti, I.R. Wijesundera, W.-K. Chu, Ion beam nanoengineering of surfaces for molecular detection using surface enhanced Raman scattering, *Mol. Syst. Des. Eng.* 7 (5) (2022) 411–421.
- [17] F. Wang, M. Zou, C. Liao, B. Li, D. Liu, J. Zhou, H. Huang, J. Zhao, C. Liu, P.K. Chu, Y. Wang, Three-dimensional printed microcantilever with mechanical metamaterial for fiber-optic microforce sensing, *APL Photonics* 8 (9) (2023).
- [18] X.X. Han, R.S. Rodriguez, C.L. Haynes, Y. Ozaki, B. Zhao, Surface-enhanced Raman spectroscopy, *Nat. Rev. Methods Primers* 1 (1) (2022) 87.
- [19] J. Purto, P. Rogin, A. Verch, V.E. Johansen, R. Hensel, Nanopillar Diffraction Gratings by Two-Photon Lithography, *Nanomaterials* 9 (10) (2019) 1495.
- [20] M. Focsan, A.M. Craciun, S. Astilean, P.L. Baldeck, Two-photon fabrication of three-dimensional silver microstructures in microfluidic channels for volumetric surface-enhanced Raman scattering detection, *Opt. Mater.* 6 (5) (2016) 1587–1593.
- [21] Q. Liu, K. Vanmol, S. Lycke, J. Van Erps, P. Vandenaebelle, H. Thienpont, H. Ottevaere, SERS using two-photon polymerized nanostructures for mycotoxin detection, *RSC Adv.* 10 (24) (2020) 14274–14282.
- [22] P.L. Stiles, J.A. Dieringer, N.C. Shah, R.P. Van Duyne, Surface-Enhanced Raman Spectroscopy, *Annu. Rev. Anal. Chem.* 1 (2008) 601–626.
- [23] B. Pokroy, S.H. Kang, L. Mahadevan, J. Aizenberg, Self-Organization of a Mesoscale Bristle into Ordered, Hierarchical Helical Assemblies, *Science* 323 (5911) (2009) 237.
- [24] C. Zhang, J. Tan, Du. Baoqiang, C. Ji, Z. Pei, M. Shao, S. Jiang, X. Zhao, Yu. Jing, B. Man, Z. Li, Xu. Kaichen, Reversible Thermoelectric Regulation of Electromagnetic and Chemical Enhancement for Rapid SERS Detection, *ACS Appl. Mater. Interf.* 16 (2024) 12085–12094.
- [25] W. Yue, T. Gong, X. Long, V. Kravets, P. Gao, Pu. Mingbo, C. Wang, Sensitive and reproducible surface-enhanced Raman spectroscopy (SERS) with arrays of dimer-nanopillars, *Sens. Actuators B Chem.* 322 (2020) 128563.
- [26] Z.-C. Ma, Y.-L. Zhang, B. Han, X.-Q. Liu, H.-Z. Zhang, Q.-D. Chen, H.-B. Sun, Femtosecond Laser Direct Writing of Plasmonic Ag/Pd Alloy Nanostructures Enables Flexible Integration of Robust SERS Substrates, *Adv. Mater. Technol.* (2017) 1600270.
- [27] Q. Yang, X. Li, L. Jiang, N. Zhang, G. Zhang, X. Shi, K. Zhang, Hu. Jie, Lu. Yongfeng, Nanopillar arrays with nanoparticles fabricated by a femtosecond laser pulse train for highly sensitive SERS, *Opt. Lett.* 40 (9) (2015) 2045–2048.
- [28] X. Yang, N. Ileri, C.C. Larson, T.C. Carlson, J.A. Britten, A.S.P. Chang, C. Gu, T. C. Bond, Nanopillar array on a fiber facet for highly sensitive surface-enhanced Raman scattering, *Opt. Express* 20 (22) (2012) 24819–24826.
- [29] Z. Yin, Y.F. Geng, Q.L. Xie, X.M. Hong, X.L. Tan, Y.Z. Chen, L.L. Wang, W.J. Wang, X.J. Li, Photoreduced AgNPs grown on femtosecond laser ablated, D-shaped fiber probe for surface-enhanced Raman scattering, *Appl. Opt.* 55 (20) (2016) 5408–5412.
- [30] J. Zhang, S. Chen, T. Gong, X. Zhang, Y. Zhu, Tapered fiber probe modified by Ag nanoparticles for SERS detection, *Plasmon.* 11 (2016) 743–751.
- [31] Du. Wei, S. Wei, Na. Li, Z. Hao, Y. Li, M. Wang, Highly sensitive fiber optic enhanced Raman scattering sensor, *Opt. Laser Technol.* 168 (2024) 109879.